International Journal of Thermal Sciences 48 (2009) 1777–1785

Contents lists available at ScienceDirect

International Journal of Thermal Sciences

journal homepage: www.elsevier.com/locate/ijts

Turbulent film condensation in the presence of non-condensable gases over a horizontal tube

Cha'o-Kuang Chen*, Yan-Ting Lin

Department of Mechanical Engineering, National Cheng Kung University, Tainan 701, Taiwan

ARTICLE INFO

Article history:
Received 4 August 2007
Received in revised form
3 December 2008
Accepted 5 February 2009
Available online 23 March 2009

Keywords:
Turbulent
Film condensation
Non-condensable gas

ABSTRACT

A numerical model is presented for studying turbulent film condensation in the presence of non-condensable gases over a horizontal tube. Inertia, pressure gradient are included in this analysis, and the influence of turbulence in the proposed two-phase model is considered. The numerical results demonstrate that a very small bulk concentration of non-condensable gas reduces the heat transfer coefficient and film thickness considerably. The local heat flux and film thickness increase as tube surface temperature decreases at any bulk concentration of non-condensable gas. Moreover, inlet velocity increases as film thickness decreases and heat flux increases, a numerical result in agreement with that obtained by Nusselt. Numerical results indicate that average dimensionless heat transfer coefficients are in good agreement with theoretical and experimental data.

1. Introduction

The original Nusselt model [1] for film-wise condensation of a quiescent vapor along an isothermal horizontal cylinder equates gravity and viscous forces and assumes a linear temperature profile across the condensate layer. For pure vapor, several studies of laminar film condensation over horizontal tubes have followed Nusselt's basic theory. At a high vapor velocity, the effect of vapor drag thins the condensate film and consequently increases surface heat transfer. Michael et al. [2] determined that under high velocity vapor flow, the condensate film is likely under turbulent regimes.

Yang and Lin [3] analyzed the effect of turbulence in a condensate film and phase-change balance equation on a horizontal cylinder. Sarma et al. [4] applied Kato's model of eddy diffusivity in a condensate film and assumed that the friction coefficient at the liquid–vapor interface is identical to that in air-flow. However, both Yang [3] and Sarma [4] utilized the Colburn analogy and the sinusoidal distribution of the vapor friction factor to determine the local vapor shear force. They did not solve the two-phase system of the film condensation. Homescu and Panday [5] employed finite difference analysis and implicit algorithm to solve coupled boundary layer equations for turbulent flow condensation on a cylinder. The inertia and convection terms are retained in the analysis. However, this study assumed that the maximum vapor boundary layer is 6 times the thickness of liquid film. Due to the thickness of the vapor boundary is much larger than that of the liquid film, this assumption may causes large vapor shear velocity and increases the heat transfer coefficient. Asbik et al. [6] solved the problem of film condensation of pure fluids outside a bundle of smooth tubes. An implicit finite difference method is used. The shear stress at the liquid–vapor interface is used as the coupling condition between the two phases. The vapor phase velocity is obtained from potential flow. Their numerical results were compared to those obtained by Michael et al. [2], demonstrating that the discrepancies between the findings was $<20\%$. For experimental condensation on a horizontal cylinder, a limited amount of experimental data exists for steam. At low-to-moderate vapor velocities, data are in good agreement with theoretical data. At high velocities, theory, which incorporates the assumption of uniform wall temperature, significantly overestimates the average heat transfer coefficient.

In numerous industrial applications, such as in the design of a condenser for refrigeration and air conditioning, condensable vapor contains non-condensable gases. Non-condensable gases are known to markedly reduce the condensation heat transfer rate. The reason for this reduction is that the condensation process effectively moves the gas to the surface where it accumulates as a gas-rich layer. The effects of non-condensable gas on steam condensation have been extensively investigated. Sparrow and Eckert [7] demonstrated that the presence of a few percent of non-condensable gas in the vapor bulk markedly reduces the surface heat transfer. Minkowycz and Sparrow [8] determined that, depending on concentration, 0.5% of air

* Corresponding author. Tel.: +886 6 2757575x62140; fax: +886 6 2342081.
E-mail address: ckchen@mail.ncku.edu.tw (C.-K. Chen).

1290-0729/$ – see front matter © 2009 Elsevier Masson SAS. All rights reserved.
doi:10.1016/j.ijthermalsci.2009.02.003

Nomenclature

c_p	specific heat [J kg^{-1} K^{-1}]
D	diameter of horizontal tube [m]
D_{ij}	mass diffusion between species i gas and species j gas in the mixture [m^2 s^{-1}]
D_m	mass diffusion of mixture [m^2 s^{-1}]
g	acceleration due to gravity [m s^{-2}]
H	parameter for coordinate transformation [m]
h_x	convective heat transfer coefficient [W m^{-2} K^{-1}] ($= q''_x/\Delta T$)
h_{fg}	latent heat due to condensation [J kg^{-1}]
i	single gas species i in the mixture
j	single gas species j in the mixture
k	thermal conductivity [W m^{-1} K^{-1}]
L_m	Prandtl mixing length
$\dot{m}''_{INT}$	mass flux at interface between mixture and liquid film [kg m^{-2} s^{-1}]
Nu	Nusselt number [$(hD)/k_L$]
N	parameter for coordinate transformation
P	pressure [N m^{-2}]
P_{IN}	static pressure [N m^{-2}]
q''_x	local heat flux [W m^{-2}] ($= -k_L(\partial T_L/\partial y)_{y=0}$)
R	universal gas constant [J kg^{-1} K^{-1}]
r	radius of horizontal tube [m]
T	temperature [K]
T_{IN}	mixture temperature in free stream [K]
T_W	wall temperature [K]
T^*	dimensionless temperature ($=(T-253)/373-253$))
U_{IN}	mixture velocity in free stream [m s^{-1}]
U^*	dimensionless tangential velocity ($=u/U_{IN}$)
u_e	tangential velocity at mixture boundary layer [m s^{-1}]
u	velocity in tangential term [m s^{-1}]
u_w	friction velocity ($= \sqrt{\tau/\rho}$) [m s^{-1}]
v	velocity in normal to condensing surface [m s^{-1}]
W	mass fraction of water vapor
W_{IN}	mass fraction of water vapor in free stream
X	molar fraction
x	tangential direction along the tube surface [m]
Y	mass fraction
y	normal direction at any point to the tube surface [m]
y^+	dimensionless coordinate ($=\rho y u_w/\mu$)

Greek symbols

δ	boundary layer thickness [m]
ρ	density [kg m^{-3}]
μ	dynamic viscosity [N s m^{-2}]
θ	angle measured from the vertical [°]
ω	transformed transverse coordinate for liquid film
η	transformed transverse coordinate for mixture flow
ξ	transformed longitudinal coordinate
τ	shear stress ($= \partial u/\partial y|_{y=0,y=INT}$) [N m^{-2}]

Subscripts

m	mixture phase
L	liquid phase
sat	saturated condition
INT	Interface
i	single gas species i in the mixture
j	single gas species j in the mixture
W	wall
x	local value
g	non-condensable gas phase
v	water vapor phase
IN	inlet (bulk) condition or free stream condition
t	turbulent condition

in steam reduces heat transfer by 50%. Slegers and Seban [9] experimentally indicated the ratio of binary mixture condensation heat transfer to Nusselt's prediction is about 20% above that obtained theoretically by Minkowycz and Sparrow [8]. Sparrow and Marshall [10] enhanced the theoretical study by considering the influence of temperature difference on the effects of non-condensable gases on heat transfer coefficients. The condensation of steam–air mixtures onto a tube in an experimental horizontal heat exchanger was analyzed by Rashtchian and Webb [11]. These studies simplified numerical model by locally replacing vapor saturation temperature in Nusselt's equation with mixture interface temperature, as solved from momentum, energy and species conservation equations. However, turbulent film condensation in the presence of non-condensable gases has received little attention in literature.

This study investigates the influence of turbulence on film condensation in the presence of non-condensable gases over a horizontal isothermal tube. The governing equations of momentum, energy and species in liquid and mixture phases are solved numerically using an implicit finite difference method. The properties of working fluid are based on the steam–air two-phase flow system.

2. Mathematical modeling

2.1. Physical model

Fig. 1 shows the physical situation. The curvilinear coordinates (x, y) are aligned along the circular tube wall surface and its normal; the corresponding velocity components are u and v. Notably, θ is the angle measured from the upper stagnation point. At a far distance from the surface, a mixture of a saturated vapor and non-condensable gas flow onto a horizontal tube cooled to, and maintained at, a uniform temperature T_W. The mixture enters with a uniform velocity U_{IN}, uniform temperature T_{IN}, uniform pressure

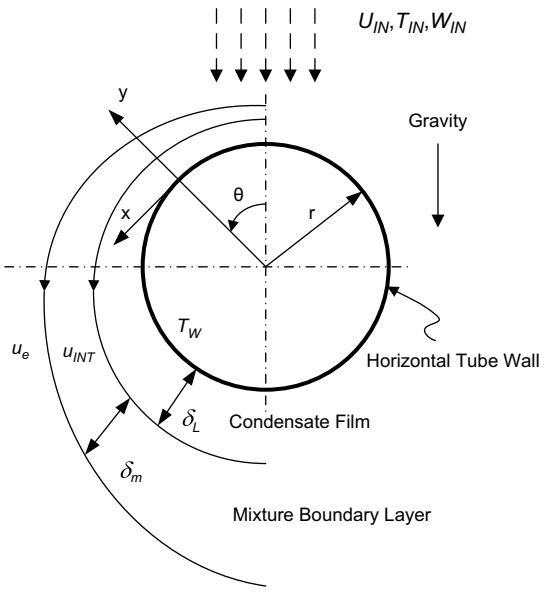

Fig. 1. Coordinate system and related physical quantities.

P_{IN}, and uniform water vapor concentration W_{IN}. As the mixture flows along the tube surface, vapor is removed from the mixture, producing a condensate layer of thickness δ on the tube.

To solve the physical situation, we made the following assumptions: (1) wall temperature is constant; (2) all physical properties are constant; (3) surface tension effect is negligible; (4) condensate film thickness is much less than the tube radius; (5) heat change downward of liquid film separation point is negligible; (6) mixture flow outside the mixture boundary layer is a potential flow; and, (7) the upward mixture is saturated and at a constant pressure.

A brief justification of these assumptions is given here. Uniform wall temperature and constant physical properties are utilized in most theoretical and experimental studies. This study employs this assumption to simplify calculations; however, the calculation procedure can be applied for variable physical properties and wall temperature, i.e., density, conductivity and viscosity.

Considerable progress has been made in the theoretical development of condensation with inclusion of the surface tension effect. According to Krupiczka [12], the surface tension effect caused by curvature of a condensate film in a simple Nusselt-type analysis on a circular cylinder can be ignored. Yang and Chen [13] also investigated the effect of surface tension on an elliptical tube caused by surface curvature and concluded that surface tension had a negligible effect for e(ellipticity) < 0.8 on the heat transfer coefficient. Yang and Hsu [14], who examined forced convection film condensation on a horizontal elliptical tube, found that the surface tension effect on the dimensionless heat transfer coefficient, $Nu/Re_L^{0.5}$, is roughly negligible under forced convection. Thus, based on these studies, this work ignores the surface tension on the liquid film.

For the potential flow assumption, since condensing thickness is of the order of a few hundredths of a millimeter, the mixture outside the boundary layer is a potential flow, and the pressure gradient in the mixture and liquid film is defined by potential function. Mixture boundary layers are larger than liquid film thickness around the tube (Fig. 2).

2.1.1. Governing equations

Based on the above mentioned assumptions, the governing equations are written in the curvilinear coordinate system as follows:

For the mixture phase:

$$\frac{\partial}{\partial x}(\rho_m u_m) + \frac{\partial}{\partial y}(\rho_m v_m) = 0 \tag{1}$$

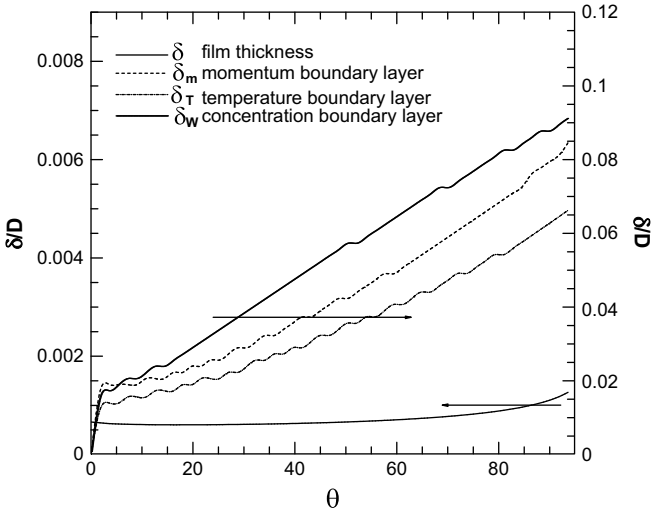

Fig. 2. Multiple thicknesses of condensate film and mixture boundary layers.

$$\frac{\partial}{\partial x}(\rho_m u_m u_m) + \frac{\partial}{\partial y}(\rho_m v_m u_m) = -\frac{\partial p}{\partial x} + \frac{\partial}{\partial y}\left[(\mu + \mu_t)_m \frac{\partial u_m}{\partial y}\right] \tag{2}$$

$$\frac{\partial}{\partial x}(\rho_m u_m c_{p,m} T_m) + \frac{\partial}{\partial y}(\rho_m v_m c_{p,m} T_m) = \frac{\partial}{\partial y}\left[(k + k_t)_m \frac{\partial T_m}{\partial y}\right] + \frac{\partial}{\partial y}\left[\rho_m (D + D_t)_m (c_{p,v} - c_{p,g}) T_m \frac{\partial W}{\partial y}\right] \tag{3}$$

$$\frac{\partial}{\partial x}(\rho_m u_m W) + \frac{\partial}{\partial y}(\rho_m v_m W) = \frac{\partial}{\partial y}\left[\rho_m (D + D_t)_m \frac{\partial W}{\partial y}\right] \tag{4}$$

For the liquid film phase:

$$\frac{\partial}{\partial x}(\rho_L u_L) + \frac{\partial}{\partial y}(\rho_L v_L) = 0 \tag{5}$$

$$\frac{\partial}{\partial x}(\rho_L u_L u_L) + \frac{\partial}{\partial y}(\rho_L v_L u_L) = -\frac{\partial p}{\partial x} + \frac{\partial}{\partial y}\left[(\mu + \mu_t)_L \frac{\partial u_L}{\partial y}\right] + g\sin\theta \tag{6}$$

$$\frac{\partial}{\partial x}(\rho_L u_L c_{p,L} T_L) + \frac{\partial}{\partial y}(\rho_L v_L c_{p,L} T_L) = \frac{\partial}{\partial y}\left[(k + k_t)_L \frac{\partial T_L}{\partial y}\right] \tag{7}$$

Eqs. (1)–(4) govern the conservation of mass, momentum, energy and concentration for the mixture, while Eqs. (5)–(7) are corresponding conservation equations for the liquid film. Notably, the second order effects of thermal diffusion, viscous dissipation, compressible heating, and diffusion-thermo have been neglected in Eqs. (3) and (4). To ensure the thermal and mechanical equilibrium in the mixture, the vapor and gas are assumed to have the same values of u, v and T at any location within the mixture.

The tangential velocity at the edge of mixture boundary layer and pressure gradient are obtained from potential flow as follows,

$$u_e = 2U_{IN}\sin\theta \tag{8}$$

$$\frac{\partial p}{\partial x} = -u_e \rho_m \frac{\partial u_e}{\partial x} \tag{9}$$

2.1.2. Boundary and compatibility conditions

At the tube wall ($y = 0$)

$$u_L = v_L = 0 \quad \text{and} \quad T_L = T_W \tag{10}$$

At the edge of the mixture boundary ($y = \delta_m$)

$$u_m = u_e,\ T_m = T_{IN} \quad \text{and} \quad W = W_{IN} \tag{11}$$

At the liquid–mixture interface ($y = \delta_L$)

$$u_m = u_L \tag{12}$$

$$\mu_L \frac{\partial u_L}{\partial y} = \mu_m \frac{\partial u_m}{\partial y} \tag{13}$$

$$\dot{m}''_{INT} = \left.\frac{\rho_m D}{(1 - W)}\frac{\partial W}{\partial y}\right|_{INT} \tag{14}$$

$$k_L \frac{\partial T_L}{\partial y} = k_m \frac{\partial T_m}{\partial y} + \dot{m}''_{INT} h_{fg} \tag{15}$$

$$\dot{m}''_{INT} = \frac{\partial}{\partial x}\left(\int_0^{\delta} \rho_L u_L dy\right) \tag{16}$$

Additionally, the equation of state (EOS) of an ideal gas mixture ($P=\rho RT$) taken from the thermodynamic tables and the thermal constraint that – the interface condition is a saturation state of the condensing vapor – yield,

$$T_{INT} = T(W_{INT}, P) \tag{17}$$

where the interface is assumed to depart negligibly from thermodynamic equilibrium, consistent with results presented elsewhere [15]. Moreover, based on the ratio of the molecular weight of air (28.96 kg/kmol) and water vapor (18.016 kg/kmol), one finally obtains

$$W = \frac{P_V}{1.61P - 0.61P_V} \tag{18}$$

where P is the mixture pressure of the air–water–vapor mixture and P_V is the partial pressure of the water vapor. If there is an interface in the boundary layer between the liquid water and the air–water–vapor mixture, and if thermodynamic equilibrium is assumed to exist at the interface, then P_V is the saturated vapor pressure of water at the interface temperature $T_{m,i}=T_{L,i}$.

The liquid film thickness is determined using a phase-change balance equation on the fact that heat transferred to tube surface equals that heat released at the liquid–mixture interface by the condensation process minus that conducted away by the liquid film. This balance subject to the boundary layer approximation gives

$$k_L\frac{\partial T_L}{\partial y}\bigg|_{y=0} = \frac{\partial}{\partial x}\left[\int_0^{\delta}\rho_L u_L\left(h_{fg}+c_{p,L}(T_{L,INT}-T_L)\right)dy\right] + k_m\frac{\partial T_m}{\partial y}\bigg|_{y=\delta} \tag{19}$$

The local Nusselt number, Nu_x, is defined as follows,

$$Nu_x = \frac{h_x D}{k_L} = \frac{q''_x D}{k_L\Delta T} = -\frac{D}{\Delta T}\frac{\partial T_L}{\partial y}\bigg|_{y=0} \tag{20}$$

Notably, the condensate film flow may happen to separation when the following condition exists:

$$\left(\frac{\partial u_L}{\partial y}\right)_{y=0} \le 0 \tag{21}$$

2.2. Turbulent model

The turbulence model based on mixing length turbulence models are applied to the liquid and mixture phases. The mixing length theory was based on Prandtl theory and successfully applied to single-phase flow. Despite its simplicity, the theory provides a remarkably adequate basis for numerous engineering applications. Thus, turbulent viscosity is expressed as

$$\mu_t = \rho L_m^2\left|\frac{\partial u}{\partial y}\right| \tag{22}$$

Furthermore, Kato et al. [16] developed the following expression for describing turbulence viscosity in both free and forced convection flows:

$$\frac{\mu_t}{\mu} = 0.4y^+\left[1-\exp\left(-0.0017\left(y^+\right)^2\right)\right] \tag{23}$$

Thus, the turbulence model in this study is acquired using Kato's mixing length model for both mixture and liquid phases. Generally, the mixing length model is valid for using in the liquid phase or single phase under the boundary layer equation. However, no reliable mixing length models exist in literature for a two-phase model. Since shear velocity of a mixture is larger than that of a condensate liquid, we assume that $u_m=0$ at $y=\delta_L$ in the mixing length model. Thus, simulation of the turbulence effect in the mixture phase is also used by the single-phase model assumption.

2.3. Mixture properties

The models for calculating the condensation process are based on the mixture properties. Therefore, the models used here have been taken from Reid et al. [17] and Martin et al. [18] The properties of the mixture density, the mixture viscosity, the mixture conductivity, the diffusion coefficient and the specific heat of the mixture are calculated using the following relations:

$$\rho_m = \sum_{i=1}^{m} Y_i\rho_i \tag{24}$$

$$\mu_m = \sum_{i=1}^{n}\frac{X_i\mu_i}{\sum_{j=1}^{n}X_j\varphi_{ij}} \tag{25}$$

$$k_m = \sum_{i=1}^{n}\frac{X_i k_i}{\sum_{j=1}^{n}X_j\psi_{ij}} \tag{26}$$

$$D_m = \frac{1-Y_i}{\sum_{j=1,\neq i}^{m}(Y_j D_{ij})} \tag{27}$$

$$c_{p,m} = \sum_{i=1}^{m} Y_i c_{p,i} \tag{28}$$

The terms of Wilke (φ_{ij}) and Mason–Saxena (ψ_{ij}) are calculated by the expressions:

$$\varphi_{ij} = \frac{1}{\sqrt{8}}\left(\frac{M_j}{M_i}\right)\left(\frac{M_i}{M_i+M_j}\right)^{0.5}\left[\left(\frac{M_i}{M_j}\right)^{0.25}+\left(\frac{\mu_i}{\mu_j}\right)^{0.5}\right]^2 \tag{29}$$

$$\psi_{ij} = \varphi_{ij}\left[1+\frac{2.41(M_j-M_i)(M_i-0.142M_j)}{(M_i+M_j)^2}\right]^2 \tag{30}$$

The physical properties of the simulation are summarized in Table 1.

2.4. Coordinate transformation

To solve the governing equations for Eqs. (1)–(6), this study introduces new coordinates ω in the liquid phase and η in the mixture phase as follows,

$$\omega = \frac{y}{\delta},\quad \xi = x = r\theta \quad and \quad \eta = \frac{y+H+(N-2)\delta}{H+(N-1)\delta} \tag{31}$$

where H and N are initial mixture boundary thickness and multipliable factor corresponded to film thickness, respectively. Thus, the region of integration is transformed into a rectangle with $\eta=1$ at the interface, $\eta=2$ at the flow edge of mixture boundary, $\omega=0$ at the tube surface, and $\omega=1$ at the interface. To ensure that the edge of the mixture boundary layer does not exceed the $\xi-\eta$ plane, H and N are set to appropriate values. Fig. 3 presents the grid system applied to model the two-phase flow domain. The detailed procedure of coordinate transformation can be found in Chen and Lin [19].

Table 1
Physical properties of the simulation.

Symbols	Values
D_{ij}	0.26^{-4} m^2 s^{-1}
D	0.014 m
U_{IN}	1 m s^{-1} or 10 m s^{-1}
T_{IN}	373 K
T_W	371.8 K ~ 353 K
ρ_L	958.4 kg m^{-3}
μ_g	2.18×10^{-5} N s m^{-2}
μ_v	1.2×10^{-5} N s m^{-2}
μ_L	2.8×10^{-4} N s m^{-2}
k_g	3.2×10^{-2} W m^{-1} K^{-1}
k_v	2.48×10^{-2} W m^{-1} K^{-1}
k_L	6.8×10^{-1} W m^{-1} K^{-1}
$c_{p,g}$	1.011×10^{3} J kg^{-1} K^{-1}
$c_{p,v}$	2.029×10^{3} J kg^{-1} K^{-1}
$c_{p,L}$	4.211×10^{3} J kg^{-1} K^{-1}
h_{fg}	2.438×10^{3} J kg^{-1}
N	1

2.5. Solution procedure

During simulations, coupled equations in Eqs. (1)–(7) are solved with their corresponding boundary conditions using the finite-volume method and a uniform staggered grid. Initial parameters of mixture-layer thickness (H and N) are selected such that they are larger than that of boundary layers δ_m, δ_T and δ_W within the mixture. Selecting H and N was via a trial-and-error procedure as δ_m, δ_T and δ_W are unknown. Concern for selecting $H = 0.5D$ and $N = 1$ is implied in this study since the H is larger than the thickest of the δ_m, δ_T and δ_W at the upper stagnation of the tube, but not excessive for avoiding unnecessary grid resolution. Additionally, $N = 1$ causes the mass conservation of Eq. (1) of the mixture flow that can be maintained in the computational domain; this avoids the computational domain of mixture flow shrinkage due to increases in film thickness. Fig. 2 presents the three boundary thicknesses and liquid film thicknesses used to guarantee that the mixture boundary layer thickness does not exceed the dimensions of the numerical domain.

The standard power law scheme [20] are utilized for the cell face in the $\xi - \eta$ and $\xi - \omega$ system. Furthermore, the couple terms are approximated using Newton–Raphson linearization. The numerical solution was based on the marching procedure. The linearized equations of coefficient matrices were created using a line successive under relaxation solver, which is equivalent to a line Gauss–Seidel solver with successive under relaxation (SUR).

Within a particular ξ station, all independent variables were compared against their corresponding values from the previous iteration.

$$\left|\frac{\phi - \phi_{old}}{\phi}\right| \leq 1 \times 10^{-7} \tag{32}$$

where ϕ is the value of the general primitive variable at a particular grid point at the current iteration, and ϕ_{old} is the value of the general primitive variable at the previous iteration level.

Because the film thickness at the upper stagnation point is unknown, the previous studies [5,14] which ignore inertial force in momentum utilized the theoretical analysis for determining the film thickness. However, in the proposed work of the steam–air condensation, the theoretical study of the film thickness at the upper stagnation point is deficient. Thus, we assume that the film thickness and both the tangential velocities of the liquid film and the mixture at the upper stagnation point are zero. Then, the first grid in the ξ direction is assumed to extremely tiny size ($\zeta = 1 \times 10^{-6}$), we calculate the film thickness of the second node in ξ direction near the upper stagnation point. If the second node is close enough to the upper stagnation point, we assume the film thickness of the second node is the initial film thickness. Finally, we obtained satisfactory result using the implicit method, as seen in Fig. 8. The implicit method have an inherent advantage over the explicit algorithms that they have no restrictions on the marching step from the point of view of numerical stability.

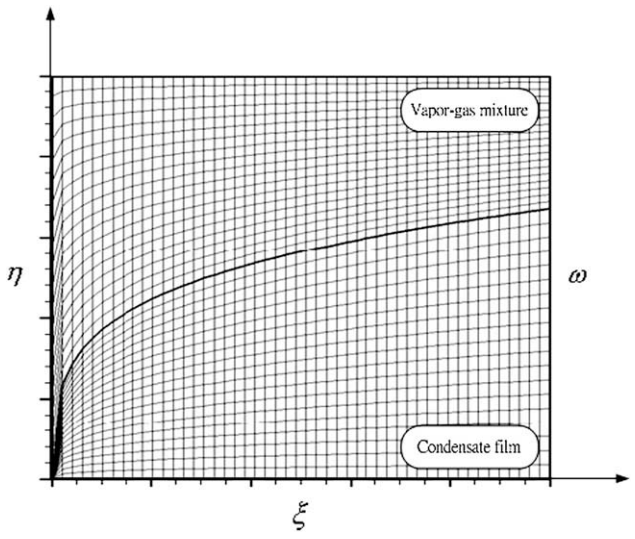

Fig. 3. Computational grid system.

3. Results and discussion

In applying the models (Fig. 1), a series of numerical simulations was performed to investigate 2D, steady state, turbulent film condensation on a horizontal tube in the presence of non-condensable gases. Two simulation results for steam–air are presented and discussed. The first simulation assessed the film thickness and heat transfer rates and their corresponding critical angles. The final simulation analyzed the average heat transfer coefficient, $Nu_{AVG}/Re_L^{0.5}$, for the effects of temperature difference and vapor concentration, and compares theoretical and experimental results.

Table 2 shows the influence of the grid size on steam condensation. The condensate film thickness, which is of the order of few hundredths of a millimeter, (Fig. 2) and truncation error increases for a number of grid points in the liquid film beyond a specific limit. The best numerical results are obtained for 201 nodes on the cylinder periphery, 121 nodes in the η direction of the mixture flow and 61 nodes in the ω direction of the liquid film. The discrepancy between numerical result and previous results can be explained by

Table 2
The effects of grid size on numerical result of $Nu/Re_L^{0.5}$.

Water vapor, $U_{IN} = 10$ m/s, $T_{IN} = 373$ K, $T_W = 363$ K, $F = 0.128$, $G = 2.05$ $Nu/Re_L^{0.5}$ = 1.022 by Fujii [27] in laminar model for dimensionless analysis $Nu/Re_L^{0.5}$ = 1.432 by Panday [5] in turbulence model for dimensionless analysis $Nu/Re_L^{0.5}$ = 0.65 – 1.95 at $G = 0.1 - 6.5$ by Mandelzweig [30] for experimental analysis				
Node numbers of ξ and ω	$\omega = 101$, $\eta = 202$	$\omega = 61$, $\eta = 122$	$\omega = 41$, $\eta = 82$	$\omega = 31$, $\eta = 62$
$\xi = 201$	1.941223	1.940155	1.9262	1.905805
$\xi = 101$	1.973212	1.961144	1.945051	1.93178
$\xi = 71$	1.993054	1.980437	1.962756	1.950597
$\xi = 51$	1.990478	2.020406	2.00029	1.979967

the fact that the previous studies employed the dimensionless laminar analysis [27] and used the fixed ratio (=6) [5] of the thickness of the mixture flow to that of the liquid film. Furthermore, in the experimental results of Fig. 10, each one of vapors shows its values of $Nu_{AVG}/Re_L^{0.5}$ for $F = 10^{-3} - 10^{3}$. Thus, we reveal that the dimensionless analysis cannot simulate all kinds of the vapors in film condensation because the film condensation depends upon the fluid properties and system pressure.

3.1. Influence of inlet conditions on local film thickness and local heat flux

This section considers the effects of inlet velocity U_{IN}, wall temperature T_W and inlet concentration W_{IN} on local film thickness and the local heat flux. The condensate film thickness gradually increases along the condensate path until separation occurs (Fig. 4). The velocity increase was rapid at the interface shear between the mixture and liquid film. Hence, the increased value of shear velocity reduces film thickness. Moreover, for a low vapor concentration, i.e., for a large value of non-condensable gas, the W_{IN} effect causes the condensate film thickness to thin. In mass transfer analysis, mass flux can be enhanced in three different ways, namely, by increasing mixture flow velocity, concentration gradient, or the binary diffusion coefficient. Hence, the reason for the marked decrease to film thickness at small vapor concentrations is that the increased vapor concentration provides additional water vapor in the mixture flow under constant system pressure.

The influence of wall temperature on film thickness was investigated at $U_{IN} = 10$ m/s; the simulate results are shown for different W_{IN} (Fig. 5). For constant system pressure and inlet saturation temperature, decreasing T_W increases ΔT. For any inlet vapor concentration, a significant increase in the slope of δ and a minor decrease in the separate location occur as T_W decreases. As indicated by Eqs. (20) and (21), a decrease in T_W results in decreased ability of the gas to absorb moisture and causes the vapor to release increased amounts of condensate film, as determined by Siow et al. [21,22]. These trends indicate that increased heat transfer is associated with decreased T_W.

Figs. 6 and 7 show the variations in local heat flux along the tube surface for different mass fractions of vapor, tube wall temperature and inlet mixture velocity. Since convection heat transfer number, h, is equal to heat flux, q'', multiplied by the temperature difference.

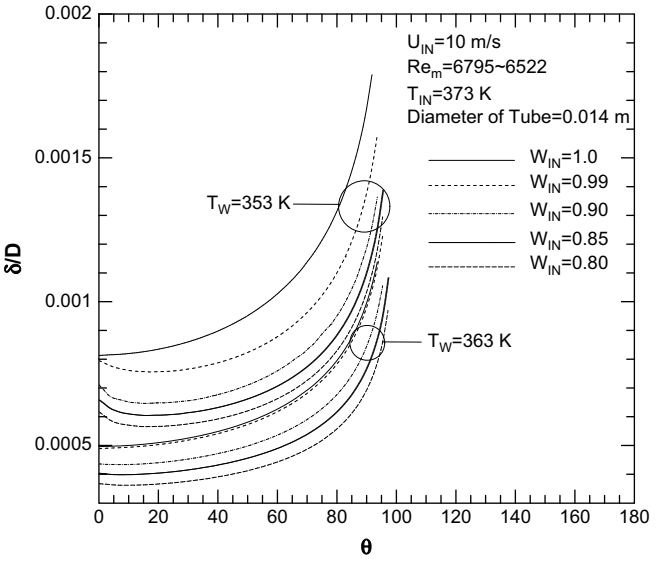

Fig. 5. Dependence of local film thickness on angle for $T_W = 353$ K and $T_W = 363$ K.

The local Nusselt number, Nu_x, has a trend that differs from that of local heat flux, q''. Thus, the local heat transfer coefficient is defined as a heat flux type for estimating heat transfer performance.

Local heat flux increases as U_{IN} increases (Fig. 6). However, local heat flux decreases as W_{IN} decreases because condensable vapor has to diffuse and convect through a vapor–gas mixture to the interface. Thus, inlet velocity of mixture flow has a significant impact on the local heat flux for steam–air film condensation.

Fig. 7 shows the effects of T_W on local heat flux from $W_{IN} = 1.0 - 0.8$. These simulate results indicate that local heat flux increases as T_W decreases at any W_{IN}, as determined by Briggs and Sabaratnam [23]. Generally, a small T_W results in increased suction, and film thickness and local heat flux should increase. The reason for this phenomena is that low T_W increases the amount of vapor to be absorbed on the cool tube. The condensate film is then created, and heat flux increases. As the film moves along the tube, the thickness is increased gradually, and the local heat flux is decreased gradually. According to Nusselt [1] and Lin [24], film thickness is inversed to local heat flux for pure condensation, with the

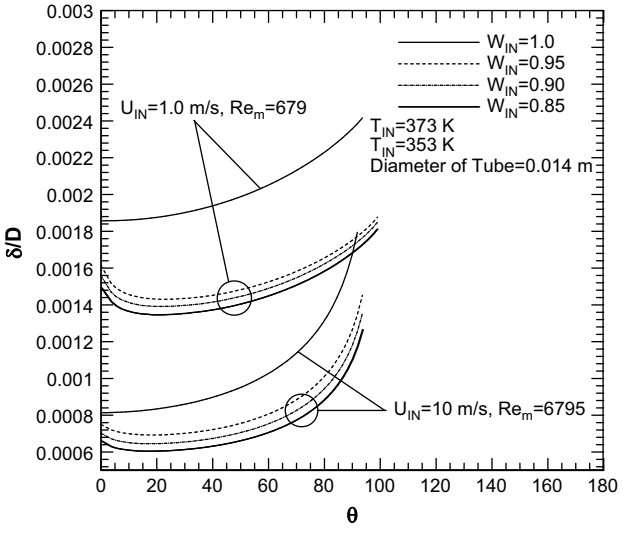

Fig. 4. Dependence of local film thickness on angle for $U_{IN} = 1$ m/s and $U_{IN} = 10$ m/s.

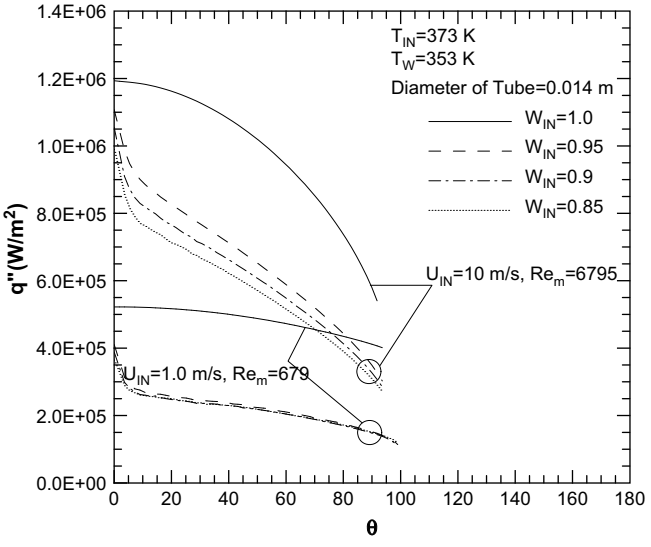

Fig. 6. Dependence of local heat flux on angle for $U_{IN} = 1$ m/s and $U_{IN} = 10$ m/s.

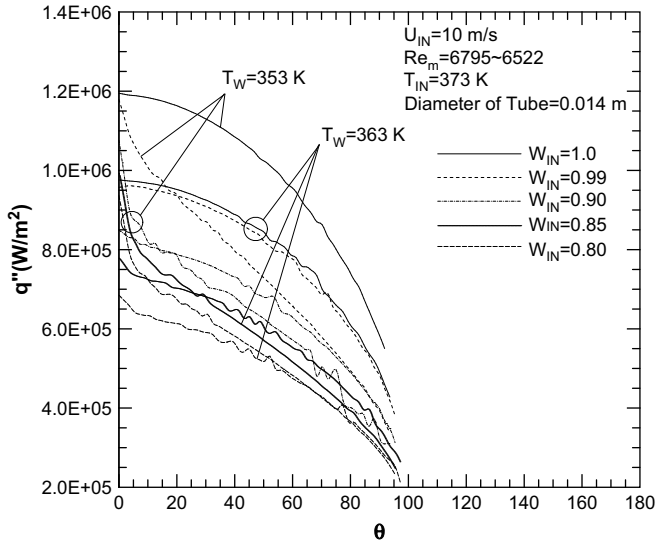

Fig. 7. Dependence of local heat flux on angle for $T_W = 353$ K and $T_W = 363$ K.

exception of the effects of temperature difference and vapor concentration. Typically, maximum local heat flux occurs at the upper stagnation point of the tube. The condensate film then grows up from the diffusion and phase change as the wall temperature is below the mixture saturation point. Thus, the condensate film will cool until it reaches wall temperature and induce a reduction in local heat flux. Moreover, the liquid film causes the heat transfer coefficient to decline due to separation from the tube.

3.2. Comparisons with theoretical and experimental results

To assess the accuracy of the proposed simulation method, numerical results are compared with those obtained by other studies theoretically or experimentally. Measured values of the film thickness profile and local heat flux are unavailable; hence, only average dimensionless heat transfer coefficients are compared.

Fig. 8 compares the variation of Nu_x with the curvilinear coordinate on the circular tube. Notably, dimensionless parameter $(Ra/Ja)^{0.25}$ is 230 in both cases. Since a quiescent and saturated vapor is utilized, the proposed model becomes free convection film condensation and approaches the value of 200 at the upper stagnation point. This value is roughly in agreement with the theoretical values of $Nu_x = 200$ with a surface tension effect [25,26]. The difference in the two simulate results can be explained by the fact that the proposed model does not consider surface tension in free condensation simulation.

For comparison of performance of the average dimensionless heat transfer coefficient, the following analytic relation obtained by Nusselt is utilized. Notably, the Nusselt-type equation [1] illustrates a linear distribution under the log scale in quiescent to moderate mixture velocities.

$$Nu_{AVG}/Re_L^{0.5} = f(F,G) \tag{33}$$

where

$$F = \frac{gD\mu_L h_{fg}}{\left[k_L U_{IN}^2 (T_{IN} - T_W)\right]} \tag{34}$$

$$G = k_L(T_{IN} - T_W)[\rho_L/(\rho_m \mu_m \mu_L)]^{0.5}/h_{fg} \tag{35}$$

Typically, F and G represent the vapor velocity and system temperature difference in experimental setting.

The effects of vapor boundary layer separation are relatively unimportant when calculating the average dimensionless heat transfer coefficient as most heat transfer occurs on the forward part of the tube before the separation point. A solution obtained by Fujii et al. [27] employed an integral treatment of the vapor boundary layer with an assumed velocity profile that avoided the separation problem, and led to the computational result

$$Nu_{AVG}/Re_L^{0.5} = Z\left(1 + 0.276F/Z^4\right)^{1/4} \tag{36}$$

where

$$Z = 0.9(1 + 1/G)^{1/3} \tag{37}$$

The proposed numerical results for steam are compared with Eq. (36) and other analytical works (Fig. 9). For an F greater than

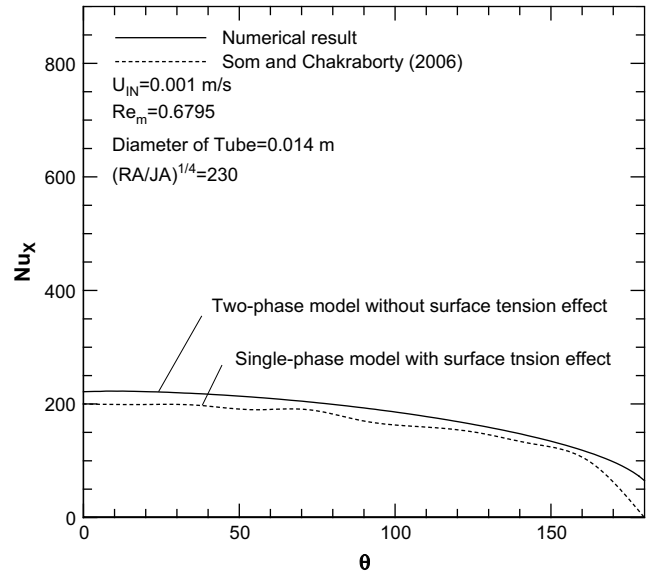

Fig. 8. Comparison of numerical result with free convection film condensation data.

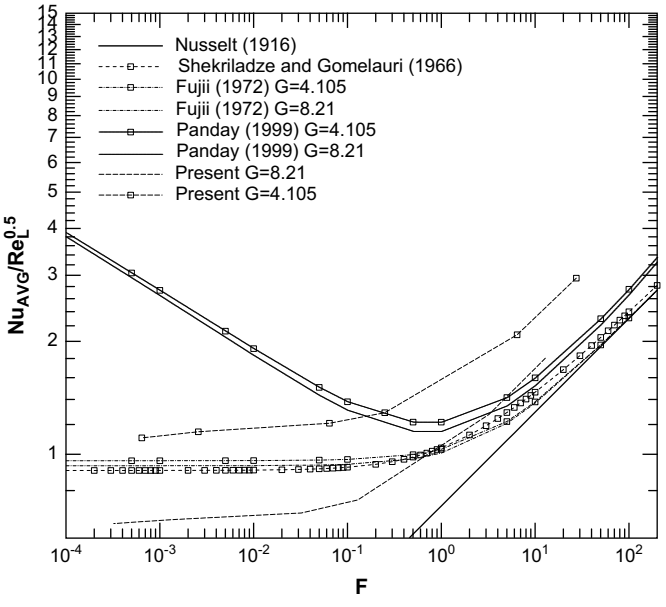

Fig. 9. Comparisons of numerical results with theoretical data.

about 1, the agreement of simulate result with previous theory is generally satisfactory at $G = 8.21$. However, at $G = 4.106$, the data in this study differ from data obtained by previous studies. This discrepancy can be explained by the turbulence model used in the proposed model. Notably, the data with low values of G generally had high values of $Nu_{AVG}/Re_L^{0.5}$ as indicated by theory. At low values of F (increased vapor velocities) obtained with steam, the computational results obtained by this study are higher than those obtained by Eq. (36) and Nusselt's study for $G = 4.106$; that is Fuji et al. [27] and other works [1,28], except for that by Homescu and Panday [5], generated their solutions using laminar film model. Furthermore, the curve obtained by Homescu and Panday [5] is higher than that in this study, and significantly larger than that in other studies as $F < 0.1$, The reason is that Homescu and Panday [5] utilized a constant ratio (=6) for mixture boundary layer thickness that is 6 times liquid film thickness. The ratio increases shear force of mixture and decrease liquid film thickness due to the increasing rate of the mixture thickness is larger than that of the film thickness. This assumption overestimate the solution when compared with experimental data for $F < 0.1$.

Fig. 10 compares computational results with early experimental data for steam. At a moderate-to-low velocity (increased values of F), all data (Fujii et al. [29], Mandelzweig [30], Nobbs [31], Lee [32] and Michael et al. [33]) are in fairly good agreement, particularly for $G = 10.26$. At high velocities, the values $Nu_{AVG}/Re_L^{0.5}$ generally lie near the center of the overall spread.

Fig. 11 presents the effect of vapor concentration on the average dimensionless heat transfer coefficient. The dimensionless average heat transfer coefficient increased by 53% and 71%, as W_{IN} increased from 0.8 to 1.0 for $T_W = 363$ K and 353 K, respectively. The increased wall temperature (small temperature difference) represents the linear relationship from $W_{IN} = 0.8 - 1.0$; however, the low wall temperature (large temperature difference) result in an increase from $W_{IN} = 0.99$ to $W_{IN} = 1.0$, and an almost flat trend from $W_{IN} = 0.8$ to $W_{IN} = 0.99$. These computational results are confirmed by Minkowycz and Sparrow [8]. Even small amounts of non-condensable gas infiltrating vapor flow may cause a significant discrepancy compared with pure steam condensation. Notably, a low T_W (high G) encourages the mixture to release additional liquid film onto the tube, and the dimensionless heat transfer coefficients decrease due to the unique combination of $Nu_{AVG}/Re_L^{0.5}$.

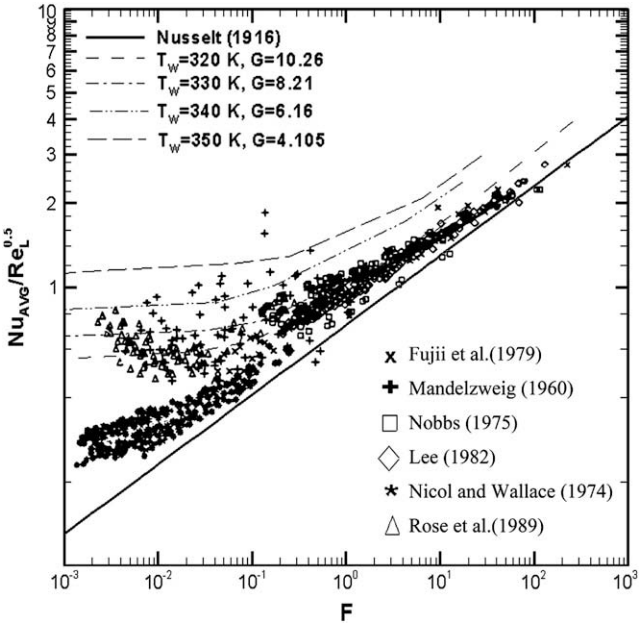

Fig. 10. Comparisons of numerical results with experimental data.

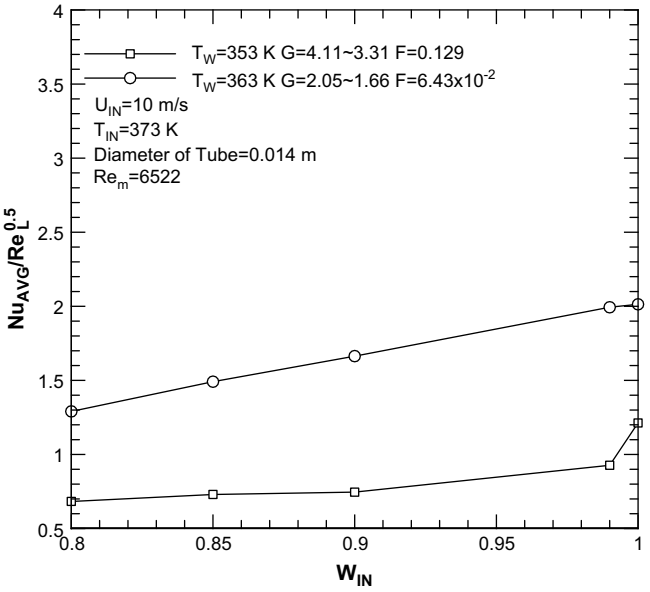

Fig. 11. Dependence of dimensionless average Nusselt number on W_{IN}.

4. Conclusion remarks

This study investigated the 2D steady state for turbulent film condensation in the presence of non-condensable gas on a horizontal tube. The effects of U_{IN}, T_W and W_{IN} on condensation results were presented and discussed separately. In the presence of non-condensable gas, local heat flux decreases markedly. As reduced vapor concentration resulted in increased heat resistance of air over the condensate film, a small W_{IN} indicated a decreasing condensate rate along the path. Thus, non-condensable gas thins the liquid film and reduces heat transfer coefficient.

Moreover, at moderate velocities, the pure vapor data for steam were generally in agreement with theoretical and experimental data obtained by other studies that incorporated the assumption of a uniform wall temperature. At the high velocities, average Nusselt numbers were distributed over the center spread of experimental data. These discrepancies may be due to the non-uniform wall temperature and fluid properties that changed in terms of temperature.

Finally, because waviness was neglected in the condensate film layer, the proposed model should be applied cautiously when tangential velocity approaches values where interfacial waves exist.

Acknowledgments

The authors would like to thank the National Science Council of the Republic of China, Taiwan, for financially supporting this research. Ted Knoy is appreciated for his editorial assistance.

References

[1] W.A. Nusselt, Die Oberflachenkondensation der Wasserdampfes, Zeitschrift Vereines deutscher ingenieure 60 (1916) 541–569.
[2] A.G. Michael, J.W. Rose, L.C. Daniels, Forced convection condensation on a horizontal tube experiments with vertical down flow of steam, ASME J. Heat Transfer 111 (1989) 792–797.
[3] S.A. Yang, Y.T. Lin, Turbulent film condensation on a non-isothermal horizontal tube-effect of eddy diffusivity, Appl. Math. Model. 29 (12) (2005) 1149–1163.

[4] P.K. Sarma, B. Vijayalakshmi, F. Mayinger, Turbulent film condensation on a horizontal tube with external flow of pure vapors, Int. J. Heat Mass Transfer 41 (3) (1998) 537–545.
[5] D. Homescu, P.K. Panday, Forced convection condensation on a horizontal tube: influence of turbulence in the vapor and liquid phases, J. Heat Transfer Trans. ASME 121 (4) (1999) 874–885.
[6] M. Asbik, A. Daif, P.K. Panday, A. Khmou, Numerical study of laminar condensation of downward flowing vapor on a single horizontal cylinder or a bank of tubes, Can. J. Chem. Eng. (1999) 54–61.
[7] E.M. Sparrow, E.R.G. Eckert, Effects of superheated vapor and noncondensable gases on laminar film condensation, AIChE J. 7 (1961) 473–477.
[8] W.J. Minkowycz, E.M. Sparrow, Condensation heat transfer in the presence of noncondensables, interfacial resistance, superheating, variable properties, and diffusion, Int. J. Heat Mass Transfer 9 (1966) 1125–1144.
[9] L. Slegers, R.A. Seban, Laminar film condensation of steam containing small concentrations of air, Int. J. Heat Mass Transfer 13 (1970) 1941–1947.
[10] E.M. Sparrow, E. Marshall, Binary gravity flow film condensation, Trans. ASME (1969) 205–211.
[11] D. Rashtchian, D.R. Webb, Condensation of steam from mixtures with air in a shell and tube exchange at atmospheric and reduced pressures, Chem. Eng. Res. Des. 157 (1987).
[12] R. Krupiczka, Effect of surface tension on laminar film condensation on a horizontal cylinder, Chem. Eng. Process. 19 (1985) 199–203.
[13] S.A. Yang, C.K. Chen, Role of surface tension and ellipticity in laminar film condensation on a horizontal elliptical tube, Int. J. Heat Mass Transfer 36 (12) (1993) 3135–3141.
[14] S.A. Yang, C.H. Hsu, Free and forced convection film condensation from a horizontal elliptical tube with a vertical plate and horizontal tube as special cases, Int. J. Heat Fluid Flow 18 (1997) 567–574.
[15] ASME Steam Tables, third ed. American Society of Mechanical Engineers, New York, 1977.
[16] H. Kato, N.N. Shiwaki, M. Hirota, On the turbulent heat transfer by free convection from a vertical plate, Int. J. Heat Mass Transfer 11 (1968) 117–1125.
[17] R.C. Reid, J.M. Prausnitz, T.K. Sherwood, The Properties of Gases and Liquids, McGraw-Hill, New York, 1977.
[18] J.M. Martin-Valdepenas, M.A. Jimenez, F. Martin-Fuertes, J.A.F. Benitez, Comparison of film condensation models in presence of non-condensable gases implemented in a CFD code, Heat Mass Transfer 41 (2005) 961.
[19] C.-K. Chen, Y.-T. Lin, Laminar film condensation from a downward-flowing steam-air mixture onto a horizontal circular tube, Applied Mathematical Modelling 33 (I 4) (2009) 1944–1956.
[20] S.V. Patankar, Numerical Heat Transfer and Fluid Flow, Hemisphere McGraw-Hill, New York, 1980.
[21] E.C. Siow, S.J. Ormiston, H.M. Soliman, Two-phase modelling of laminar film condensation from vapor–gas mixtures in declining parallel-plate channels, Int. J. Therm. Sci. 46 (5) (2007) 458–466.
[22] E.C. Siow, S.J. Ormiston, H.M. Soliman, A two-phase model for laminar film condensation from steam–air mixtures in vertical parallel-plate channels, Heat Mass Transfer 40 (5) (2004) 365–375.
[23] A. Briggs, S. Sabaratnam, Condensation of steam in the presence of air on a single tube and a tube bank, Int. J. Energ. Res. 27 (4) (2003) 301–314.
[24] Y.T. Lin, S.A. Yang, Turbulent film condensation on a nonisothermal horizontal tube, J. Mech. 21 (4) (2005) 235–242.
[25] S.K. Som, S. Chakraborty, Film condensation in presence of non-condensable gases over horizontal tubes with progressively increasing radius of curvature in the direction of gravity, Int. J. Heat Mass Transfer 49 (2006) 594–600.
[26] S. Mukhopadhyay, S.K. Som, S.A. Chakraborty, generalized mathematical description for comparative assessment of various horizontal polar tube geometries with regard to external film condensation in presence of non-condensable gases, Int. J. Heat Mass Transfer 50 (17–18) (2007) 3437–3446.
[27] T. Fujii, H. Uehare, C. Kurata, Laminar filmwise condensation of flowing vapor on a horizontal tube, Int. J. Heat Mass Transfer 15 (1972) 235–246.
[28] I.G. Shekriladze, V.I. Gomelauri, Theoretical study of laminar film condensation of flowing vapor, Int. J. Heat Mass Transfer 9 (1966) 581–591.
[29] T. Fujii, H. Honda, K. Oda, Condensation of steam on a horizontal tube-the influence of oncoming velocity and thermal condition at the tube wall, American Society of Mechanical Engineers, Applied Mechanics Division, AMD, (1979) 35–43.
[30] S.I. Mandelzweing, The effect of vertically downward velocity on the heat transfer from a steam–nitrogen mixture condensing on a horizontal cylinder, MSc Thesis, Queen Mary College, University of London, United Kingdom, 1960.
[31] D.W. Nobbs, The effect of downward vapor velocity and inundation on the condensation rates on horizontal tubes and tube banks, PhD Thesis, University of Bristol, United Kingdom, 1975.
[32] W.C. Lee, Filmwise condensation on a horizontal tube in presence of forced convection and non-condensing gas, PhD Thesis, Queen Mary College, University of London, United Kingdom, 1982.
[33] A.G. Michael, J.W. Rose, L.C. Daniels, Forced convection condensation on a horizontal tube – experiments with vertical downflow of steam, Journal of Heat Transfer, Transactions ASME 111 (3) (1989) 792–797.